Green Energy, Environment and Sustainable Development
C. Wang et al. (Eds.)

doi:10.3233/ATDE230315

Visualization Experiment of Condensation in Expansion and Contraction Microchannels

Weihong LIU[1] and Xiang LING
School of Mechanical and Power Engineering, Nanjing Tech University, Nanjing 211816, Jiangsu, China

Abstract. This paper conducted visualization experiments on condensation heat transfer of three different types of microchannels with periodic expansion and contraction structures. The difference in microchannels lies in the relative lengths of the expansion and contraction sections. Using pure steam as the experimental working fluid, the visualization experiment observed dropwise condensation, annular condensation, injection condensation, and intermittent condensation. Besides, different phenomena of "gasping" and "breakpoint antedisplacement" were observed in the injection flow, which was different from those in straight microchannels. In addition, a two-phase flow map was established for three kinds of microchannels. The findings indicated that under the same steam mass flux, increasing the length of the expansion section of the microchannels and reducing the length of the contraction section led to an augmented annular flow area within the microchannels. Increasing the length of the microchannel expansion section and reducing the length of the contraction section are beneficial for reducing the frictional pressure drop of vapor condensation, but maintaining the same length of the microchannel expansion section and contraction section can achieve the best condensation heat transfer effect.

Keywords. Microchannel, two-phase flow, condensation, heat transfer

1. Introduction

The development of industry and technology often leads to an increase in energy consumption and damage to the ecological environment. Developing efficient and strengthened heat exchange components and methods can not only improve the efficiency of heat exchange systems and reduce energy consumption but also improve the recycling and utilization rate of some waste resources and reduce ecological environment damage. In this context, microscale heat transfer [1-3] and phase change heat transfer [4-6] have received extensive research. The condensation heat transfer in microchannels [7-10] is a more efficient heat transfer method, and the process and mechanism of two-phase flow heat transfer are more complex. Existing research on condensation two-phase flow and heat transfer in microchannels is mostly found in straight channel structures with equal cross-sections. Therefore, visualization experiments were conducted on three different structures of expansion and contraction

[1] Corresponding Author, Weihong LIU, School of Mechanical and Power Engineering, Nanjing Tech University, Nanjing 211816, Jiangsu, China; Email: lwhdeyouxiang@163.com.

microchannels in this work, and the effects of expansion and contraction structures on the condensation two-phase flow pattern, pressure drop, and heat transfer were analyzed.

2. Experimental System

2.1. Experimental Setup

Figure 1 depicts the condensation visualization experimental system and process, which mainly consists of a microchannel heat exchange system, a cooling water circulating system, a visualization system, and a data acquisition system.

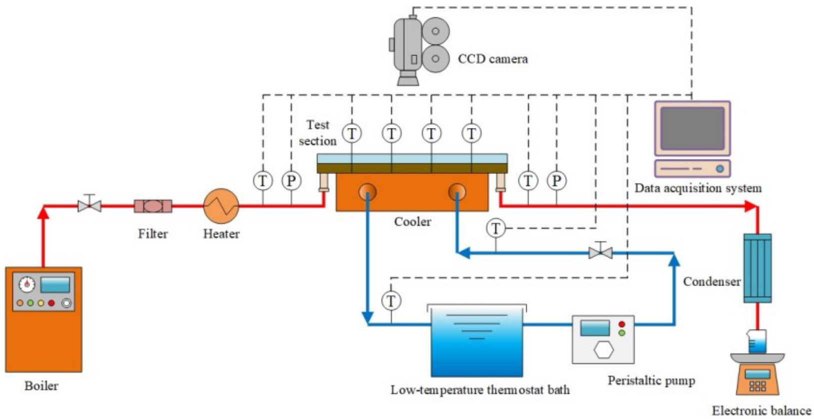

Figure 1. Schematic diagram of the visual experimental setup for condensation.

2.2. Expansion and Contraction Microchannel Heat Sink

The cross-section style of the microchannel is the continuous gradual expansion and contraction of the walls on both sides, and the two-dimensional structure diagram of a single microchannel is shown in Figure 2. As shown in the figure, when considering only the influence of the expansion and contraction structure on the flow and heat transfer processes without involving the depth of the channel, the parameters available for research include the maximum width H of the channel, the rib height e, and the length L_1, L_2, and L of the expansion and contraction section. Therefore, three different structures of microchannels were designed in this experiment, and the detailed structural parameters are shown in Table 1.

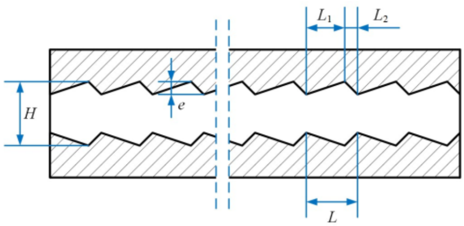

Figure 2. Geometry size of the microchannel.

Table 1. Feature size of the microchannels.

	H/μm	e/μm	L_1/μm	L_2/μm
No. 1	500	100	200	200
No. 2	500	100	100	300
No. 3	500	100	300	100

2.3. Data Reduction

Condensation heat transfer of microchannel can be calculated according to heat absorption of cooling water.

$$Q = m_c c_p \left(T_{co} - T_{ci}\right) \tag{1}$$

The vapor quality at the microchannel inlet can be approximately considered as 1, and the outlet quality is calculated according to the condensation heat transfer.

$$x_{out} = x_{in} - \frac{Q}{m_v h} \tag{2}$$

The average condensation heat transfer coefficient in the microchannel is:

$$h = \frac{Q}{A \Delta T_m} \tag{3}$$

3. Results and Discussion

Similar to the condensation flow phenomenon in conventional flat silicon-based microchannels, the pure vapor condensation flow in the expansion and contraction microchannels presents four different flow forms along the flow direction, namely dropwise condensation, annular condensation, injection condensation, and intermittent condensation.

Figure 3 shows the experimental images of injection flow captured at different times in the No. 1 microchannel. The injection flow morphology captured in the other expansion and contraction microchannels is similar to it. The experimental observation position is 32 mm-35 mm away from the entrance of the microchannel, and the input steam mass flux is 24.4 kg/(m^2·s). The injection flow is a periodically changing form during the vapor condensation process within the microchannel, which can be divided into the jet front end and the neck. As the liquid film on both sides of the jet front end continues to thicken, the forward inertial force of the gas phase core is not enough to overcome the tendency of the liquid phase fusion on both sides of the jet front end. At this time, the phenomenon of “neck contraction” appears. After the liquid film fusion, the jet neck breaks, and the jet front end forms an aeroelastic separation and continues to move forward. Under further condensation and surface tension, the slug gradually develops into a small bubble, while a new jet front and neck form, completing the periodic process of injection flow.

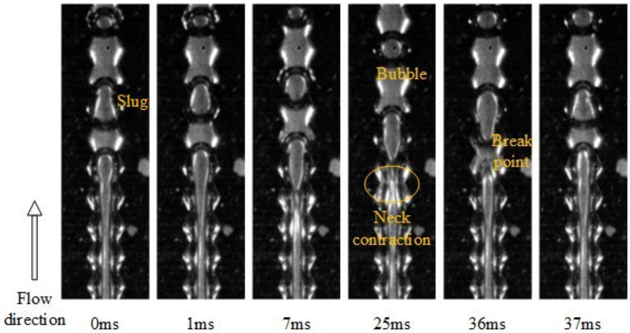

Figure 3. Injection flow pattern of vapor condensation in microchannel No. 1.

During the experiment, it was found that the frequency and breakpoint position of the injection flow was mainly influenced by the steam flow rate. As the steam flow rate increases, the breakpoint position of the injection flow moves closer and the injection flow frequency also increases. Due to the influence of the expansion and contraction structure, the contraction section of the expansion and contraction unit hinders the forward movement of the jet front end, suppresses the advancement of the injection flow, and thus affects the frequency of the injection flow. Specifically, at lower steam flow rates, when the jet neck is about to fracture, the forward movement of the jet front end is suppressed and rebound occurs, causing the neck that is about to contract and fracture to expand, thereby forming a liquid film wave phenomenon similar to "gasping", as depicted in Figure 4.

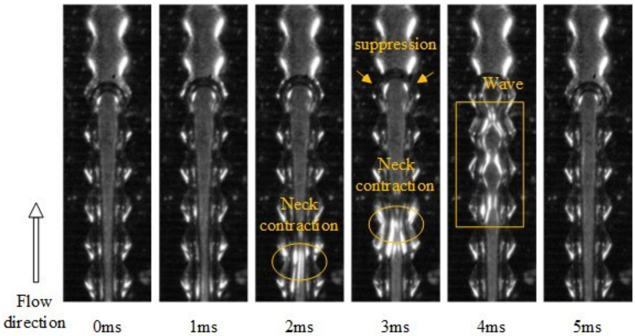

Figure 4. The gasping of injection flow pattern in microchannel No. 1.

Furthermore, due to the suppressive effect of the contraction section of the expansion and contraction unit, at lower steam flow rates, the position where injection flow occurs in the expansion and contraction microchannel is higher, and the steam quality is also higher. Therefore, the volume fraction of the jet front end occupying the channel space is larger, which is more susceptible to the influence of the channel structure shape, as shown in Figure 5. At 4 ms, in addition to the unique necking of the injection flow, due to the expansion and contraction structure, the front end of the jet also contracts, and the final breakpoint position appears at the contraction point before the necking. The small bubble directly generated after the jet are also different from the slug in Figure 3. The response time of this injection process is faster than that of the conventional injection process in Figure 3 so that the bubble fracture is completed within 1 ms after the obvious neck contraction phenomenon and the contraction of the jet front end is observed.

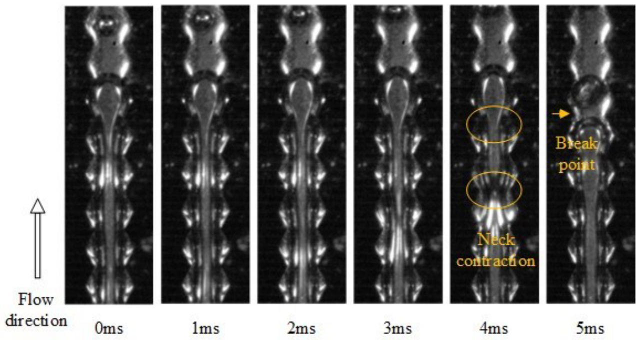

Figure 5. Breakpoint antedisplacement of injection flow pattern in microchannel No. 1.

Figure 6 shows the transformation relationship of injection flow patterns in three microchannels, plotted using steam quality and vapor mass flux as coordinates. The lines depicted within the figure represent the experimental conditions for the occurrence of injection flow in the microchannel. The area above the lines delineates the experimental parameters for the occurrence of dropwise flow and annular flow in the microchannel, and the area below the lines identifies the experimental parameters for the occurrence of intermittent flow in the microchannel. The results show that the higher the vapor mass flux, the smaller the quality of the vapor when injection flow occurs. This indicates that the injection flow takes place rearward in the microchannel, resulting in an increased area allocated for the annular flow within the microchannel. Furthermore, through a comparison of the map depicting flow patterns in two-phase systems, it is apparent that when subjected to identical vapor mass flux rates, the No. 2 microchannel is more likely to form injection flow, while the No. 3 microchannel has the smallest steam quality when injection flow occurs, indicating that increasing the length of the expansion section of the microchannels and reducing the length of the contraction section can better maintain the annular flow in the microchannels.

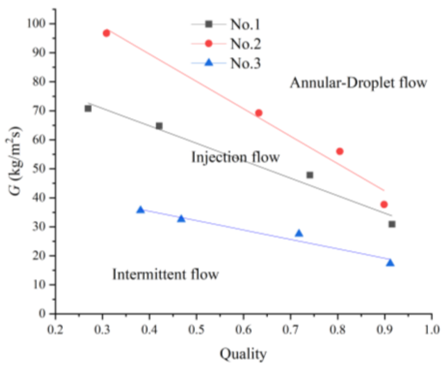

Figure 6. Two-phase flow patterns map for microchannels.

Figure 7 illustrates the frictional pressure drop of vapor condensation in three microchannels under varying vapor mass flux conditions. The findings reveal that an increase in vapor mass flux leads to a corresponding increase in the frictional pressure drop, which is attributed to the rise in two-phase flow velocity within the microchannel, ultimately resulting in a surge in wall frictional resistance. It is worth mentioning that at low vapor mass flux, the two-phase frictional pressure drop remains closely comparable in the three microchannels. However, as vapor mass flux rises, the No. 2 microchannel displays a higher frictional pressure drop of vapor condensation, while the No. 3 microchannel features a relatively lower two-phase frictional pressure drop. Thus indicating that lengthening microchannel expansion sections and decreasing contraction section length can help mitigate the frictional pressure drop.

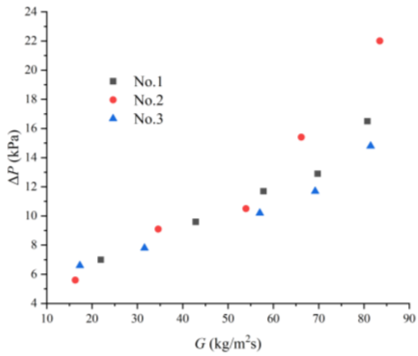

Figure 7. Frictional pressure drop of vapor condensation in microchannels.

As depicted in Figure 8, the microchannel's expansion and contraction structure significantly impacts the average condensation heat transfer coefficient. The study's findings reveal that the two-phase flow's average condensation heat transfer coefficient enhances with increasing steam mass flux. This improvement is due to the gas-liquid two-phase flow's increased velocity, promoting the heat and mass transfer rate between the steam and wall. Microchannel No. 1 demonstrates the most effective heat transfer characteristics. Additionally, microchannel No. 2's average condensation heat transfer coefficient surpasses that of No. 3, indicating that maintaining equal lengths of expansion and contraction sections in the microchannel promotes condensation heat transfer improvement.

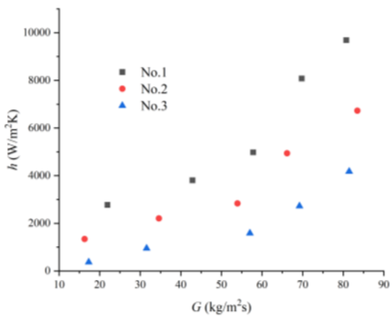

Figure 8. Average heat transfer coefficient of vapor condensation in microchannels.

4. Conclusions

In this paper, steam condensation visualization experiments were conducted on three different structures of expansion and contraction microchannels, and the following conclusions were obtained:

(1) Similar to flat microchannels, pure steam condensation in expansion and contraction microchannels also exhibits four condensation forms, such as dropwise condensation, annular condensation, injection condensation, and intermittent condensation. However, due to the influence of the expansion and contraction structure, the injection flow exhibits the characteristics of "gasping" and "breakpoint antedisplacement".

(2) Under the same steam mass flux, increasing the length of the microchannel expansion section and reducing the length of the contraction section can increase the annular flow area within the microchannel.

(3) Increasing the length of the microchannel expansion section and reducing the length of the contraction section is beneficial for reducing the frictional pressure drop of vapor condensation, but maintaining the same size of the microchannel expansion section and contraction section can achieve the best condensation heat transfer effect.

References

[1] Tuckerman DB, Pease RFW. High-performance heat sinking for VLSI. IEEE Electron Device Letters. 1981;2(5):126-9.

[2] Yong JQ, Teo CJ. Mixing and heat transfer enhancement in microchannels containing converging-diverging passages. Journal of Heat Transfer. 2014;136(4).

[3] Hajji H, Kolsi L, Ghachem K, Maatki C, Hussein AK, Borjini MN. Numerical study of heat transfer and flow structure over a microscale backstep. Alexandria Engineering Journal. 2021;60(3):2759-68.

[4] Al-Zaidi AH, Mahmoud MM, Karayiannis TG. Condensation flow patterns and heat transfer in horizontal microchannels. Experimental Thermal and Fluid Science. 2018;90:153-73.

[5] Jiang R, Ma X, Lan Z, Bai Y, Bai T. Visualization study of condensation of ethanol-water mixtures in trapezoidal microchannels. International Journal of Heat and Mass Transfer. 2015;90:339-49.

[6] Liang G, Mascarenhas N, Mudawar I. Analytical and experimental determination of slug flow parameters, pressure drop and heat transfer coefficient in micro-channel condensation. International Journal of Heat and Mass Transfer. 2017;111:1218-33.

[7] Al-Bakri BAR, Ricco P. Condensation heat transfer coefficient for rectangular multiport microchannels at high ambient temperature. International Journal of Heat and Mass Transfer. 2019;138:866-78.

[8] Chu W, Chen C, Liao Y, Wang C. A novel micro-channel heat sink with trapezoid drainage for enhancing condensation heat transfer of dielectric fluid. Experimental Thermal and Fluid Science. 2019;106:11-24.

[9] Sheng W, Li X, Wang R, Dang C, Song M. Condensate drainage on slit or louvered fins in microchannel heat exchangers for anti-frosting. Energy and Buildings. 2020;223:110215.

[10] Kim S, Mudawar I. Review of databases and predictive methods for pressure drop in adiabatic, condensing and boiling mini/micro-channel flows. International Journal of Heat and Mass Transfer. 2014;77:74-97.